Applied Physics Letters ARTICLE scitation.org/journal/apl

Redshift and amplitude increase in the dielectric function of corundum-like α-$(Ti_xGa_{1-x})_2O_3$

Cite as: Appl. Phys. Lett. **122**, 092101 (2023); doi: 10.1063/5.0139725
Submitted: 22 December 2022 · Accepted: 10 February 2023 ·
Published Online: 27 February 2023

View Online Export Citation CrossMark

Elias Kluth,[1,a)] Michael Fay,[2] Christopher Parmenter,[2] Joseph Roberts,[3] Emily Smith,[2] Craig Stoppiello,[2] Fabien Massabuau,[4] Rüdiger Goldhahn,[1] and Martin Feneberg[1]

AFFILIATIONS

[1]Institut für Physik, Otto-von-Guericke-Universität Magdeburg, Universitätsplatz 2, 39106 Magdeburg, Germany
[2]Nanoscale and Microscale Research Centre (nmRC), University of Nottingham, University Park, Nottingham NG7 2RD, United Kingdom
[3]School of Engineering, The University of Liverpool, Liverpool L69 3GH, United Kingdom
[4]Department of Physics, SUPA, University of Strathclyde, Glasgow G4 0NG, United Kingdom

[a)]Author to whom correspondence should be addressed: elias.kluth@ovgu.de

ABSTRACT

Redshift of the absorption onset and amplitude increase in the ultraviolet complex dielectric function (DF) of corundum-like α-$(Ti_xGa_{1-x})_2O_3$ with increasing Ti content is presented. α-Ga_2O_3 thin film samples alloyed with Ti up to $x = 0.61$ are grown from plasma enhanced atomic layer deposition. They are characterized by ultraviolet spectroscopic ellipsometry, transmission electron microscopy, and x-ray photoelectron spectroscopy (XPS). The samples are shown to be crystalline up to $x = 0.053$. Ellipsometry is employed to obtain the ordinary complex DF, where the absorption onset shows a strong red shift with increasing Ti content as well as an increase in amplitude, which is associated with a successive take over of Ti related 3d-states in the density-of-states. Valence band XPS results lead to the conclusion that the strong red shift in the absorption onset with increasing Ti content is mainly due to conduction band lowering and less from the valence band.

Ultra-wide bandgap semiconductors are promising materials for applications such as power electronics, solar-blind UV detectors,[1] or chemical and biological sensing devices.[2] Ga_2O_3, in particular, plays an important role here since it is already used successfully in, e.g., power electronics or solar-blind UV detectors.[1,3–5] At least four different poly-types open up a wide range of possible applications. The stable form of Ga_2O_3 is the monoclinic β-phase ($C2/m$), but it also crystallizes in the cubic γ-($Fd\bar{3}m$) and δ-phase ($Ia\bar{3}$), the orthorhombic ϵ-($P6_3mc$) and κ-phase ($Pna2_1$), and the rhombohedral corundum-like α-phase ($R\bar{3}c$).[4] The α-phase especially offers the possibility of bandgap engineering by replacing the group III element fractionally, e.g., by In and/or Al.[6–9] Titanium oxide also has a metastable corundum-like crystal structure. While it stabilizes as TiO_2 in the tetragonal rutile ($P4_2/mnm$), anatase ($I4_1/amd$), or the orthorhombic brookite ($Pbca$) phase,[10] it also occurs as α-Ti_2O_3 in the corundum-like rhombohedral phase ($R\bar{3}c$).[11] α-Ti_2O_3 is a narrow-gap semiconductor/semi-metal with a bandgap only between 0 and 0.1 eV.[12–16] Hence, alloying α-Ti_2O_3 with α-Ga_2O_3 (fundamental indirect gap at 5.0–5.4 eV,[17–19] first direct gap at ≈ 5.6 eV)[20,21] yields the possibility to tune the bandgap from the UV spectral range to basically zero. Even though α-Ti_2O_3 has been arousing increasing interest lately,[22–25] only scarcely reports on the $(Ti_xGa_{1-x})_2O_3$ alloy system can be found. There are some theoretical calculations on β-Ga_2O_3 doped by Ti[26] as well as experimental investigations[27,28] and reports on corresponding optical properties. For example, Liu *et al.*[29] found a red shift of the absorption edge by ellipsometry. Also, Ti doped ϵ-Ga_2O_3 was investigated.[30] However, no comparable results on α-$(Ti_xGa_{1-x})_2O_3$ are available so far.

Therefore, in this work, we study spectroscopic ellipsometry on α-$(Ti_xGa_{1-x})_2O_3$ to obtain the optical properties in form of the dielectric function, which is supported by transmission electron microscopy (TEM) and X-ray photoelectron spectroscopy (XPS) results.

We investigated six thin film samples consisting of α-$(Ti_xGa_{1-x})_2O_3$ on 0.25° miscut c-plane (0001) sapphire substrates, grown by plasma enhanced atomic layer deposition (ALD). More details on the growth process are found elsewhere.[31] In that study, the Ti fraction x was obtained by Rutherford backscattering spectrometry (RBS). It was found that x varies from 0 up to 0.61 from sample to

sample. Up to $x = 0.053$, the samples are reported to have the corundum-like crystal structure ($R\bar{3}c$); for higher x, they are amorphous, i.e., no x-ray diffraction (XRD) signal from the layer could be detected in $2\theta - \omega$ scans. The layer thickness varies in the range from 13 to 29 nm. All samples including some of the experimental results of this work are listed in Table I.

In this study, ultraviolet (UV) spectroscopic ellipsometry was employed to investigate the optical properties of α-$(Ti_xGa_{1-x})_2O_3$ in the form of the complex dielectric function $\varepsilon(\hbar\omega)$. Additional observations by TEM allowed to verify the film thickness, crystalline properties, and layer homogeneity. Finally, XPS was used to investigate the structure of the valence band.

UV ellipsometry was performed in the spectral range from 0.5 to 6.5 eV using a scanning variable-angle spectroscopic ellipsometer based on a grating monochromator equipped with an autoretarder. The measurements were taken at angles of incidence Φ of 50°, 60°, and 70° for each sample. Even though the samples are only 10 to 30 nm thick, they are measurable by ellipsometry with high accuracy in contrast to normal incidence transmission experiments. Spectroscopic ellipsometry provides the ellipsometric angles Ψ and Δ, which correspond to the amplitude ratio and the phase shift of the parallel and perpendicularly polarized components of the reflected light to the plane of incidence. For the analysis of the experimental data, we apply the approach[20] used to study c-plane α-Ga_2O_3 on a c-plane Al_2O_3 substrate. A multi-layer model leads to the complex dielectric function (DF) $\varepsilon(\hbar\omega)$. The model contains the c-plane α-Al_2O_3 substrate, which is taken into account anisotropically, based on a model dielectric function from Malitson.[32] On top of that, the α-$(Ti_xGa_{1-x})_2O_3$ layer follows, and the surface is defined by an effective medium approximated layer (EMA) using Bruggeman's formalism[33] to take into account surface roughness and further possible surface effects like band-bending, adsorption of organic molecules, or a variation of the composition over the top few nm. By modeling for the Fabry–Pérot oscillations, the thicknesses of the epitaxial layer and the EMA can be determined (see Table I). In the α-$(Ti_xGa_{1-x})_2O_3$ layer, which is our layer of interest, a so-called point-by-point fit (pbp) was used in the final analysis step, which fitted the calculated optical response of the multi-layer model to the experimental Ψ and Δ until the best match was achieved, by varying ε_1 and ε_2 at every energy $\hbar\omega$. As a result, we obtain the pbp-DF with real $\varepsilon_1(\hbar\omega)$ and imaginary parts $\varepsilon_2(\hbar\omega)$ corresponding to the square of the refractive index and the absorption, respectively. A more detailed discussion on the analysis of the ellipsometric experimental data along with a justification that the pbp-DF fulfills the Kramers–Kronig relationship (Fig. S1) can be found in the supplementary material. It should be noted that for the crystalline samples, only the ordinary DF, i.e., with the electric field vector perpendicular to the c-axis of the crystal, is attainable because of the c-plane orientation of the samples. There are certain differences between the ordinary DF of an anisotropic analysis and an isotropic one attained from c-plane samples as done here (in the α-$(Ti_xGa_{1-x})_2O_3$ layer).[34] Therefore, an anisotropic evaluation is often used for c-plane samples in ellipsometric investigations.[9,35,36] However, this is not necessary here, due to the very small thickness of the samples, which, combined with the choice of the angle of incidence, reduces the influence of the extraordinary component in our measurements to nearly zero and, thus, gives us a perfect agreement between measurement data and model. In the case of amorphous samples, no anisotropy is expected, and the pbp-DF will represent the true optical response of the system.

TABLE I. Roughness (r) and thickness (d) for all six investigated α-$(Ti_xGa_{1-x})_2O_3$ samples from ultraviolet spectroscopic ellipsometry (UVSE) and transmission electron microscopy (TEM) are listed. UVSE errors from numerical fitting are below 1% for all samples except the $x = 0.61$, and their corresponding maximum TEM error, from image analysis, is 6%. RMS roughness and x values by RBS from Barthel *et al.*[31] are given as well supplemented by the x values determined from XPS.

x_{RBS}	x_{XPS}	RMS	r		d		$d + r$	
		nm	nm		nm		nm	
Ref. 31		Ref. 31	UVSE	TEM	UVSE	TEM	UVSE	TEM
0.0	0.0	0.71	4.7	9.9	23.9	18.7	28.6	28.6
0.037	0.067	0.49	5.5	4.6	15.9	16.7	21.4	21.3
0.053	0.045	0.30	5.7	6.8	14.7	13.8	20.4	20.6
0.128	0.093	0.22	5.3	7.1	15.1	14.9	20.4	22.0
0.231	0.170	0.19	6.4	⋯	12.7	⋯	19.1	⋯
0.61	0.483	0.16	8.8	5.7	4.5	13.1	13.3	18.8

The samples were observed in cross section by bright field transmission electron microscopy (BF-TEM) and high angle annular dark field scanning transmission electron microscopy (HAADF-STEM) using a Tecnai Osiris (for the sample with $x = 0$, HAADF-STEM), an FEI Titan operated ($x = 0.037$, HAADF-STEM), and a JEOL 2100F ($x \geq 0.053$, BF-TEM) operated at 200 kV. The samples with $x = 0.0$ and $x = 0.037$ were prepared for imaging using standard mechanical grinding followed by Ar^+ ion milling procedure, while the samples with $x \geq 0.053$ were prepared using focused ion beam (FIB) in an FEI Quanta200 3D DualBeam and Zeiss Crossbeam 550. In the case of the sample with $x = 0.231$, FIB lift out for TEM analysis was attempted, but it was not successful, and, thus, no results can be provided for this one.

XPS was performed using a Kratos AXIS ULTRA LiPPS instrument with a monochromated Al Kα X-ray source (1486.6 eV) operated at 10 mA emission current and 12 kV anode potential (120 W). Spectra were acquired with the Kratos VISION II software. The analysis chamber pressure was $<6 \times 10^{-9}$ mbar. A survey scan was acquired with a binding energy range from 1400 to −5 eV, a step size of 0.5 eV, a pass energy of 80 eV, and a sweep time of 20 min. High resolution scans of detected elements and the valence band were performed at a pass energy of 20 eV, a step size of 0.1 eV, and a sweep time of 10 min. Spectra were converted into VAMAS format for further analysis (CasaXPS version 2.3.24 PR1.0).

Exemplarily, the experimental Ψ and Δ in comparison to the pbp-fit for the sample having $x = 0.037$ are illustrated in Fig. 1, showing that the fit and data are in excellent agreement.

The thicknesses of α-$(Ti_xGa_{1-x})_2O_3$ (d) and of the Bruggeman EMA layers (r) found from modeling Ψ and Δ are compared to corresponding TEM results in Table I. The uncertainty for the ellipsometry thicknesses and roughnesses is below 1% for all samples except the sample with x = 0.61. The maximum TEM uncertainty is at about 6%. Note here that the Ellipsometry uncertainties only are the numerical mean squared error, which is minimized using a Levenberg-Marquardt algorithm while fitting the multi-layer model mentioned earlier onto the experimental data. The TEM error origins from obtaining thickness measurements of several images, which will by far

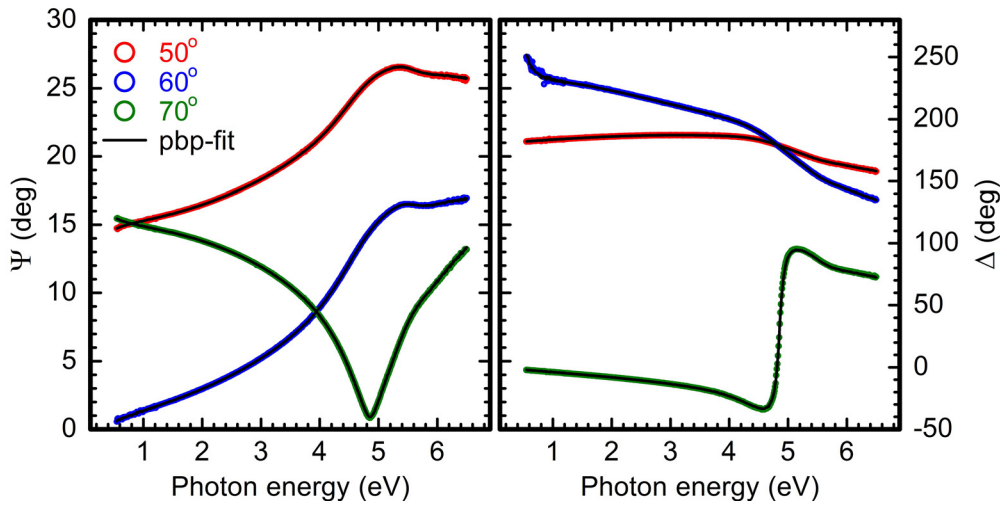

FIG. 1. The ellipsometric angles Ψ and Δ measured by spectroscopic ellipsometry in the ultraviolet and visible spectral range for the α-$(Ti_xGa_{1-x})_2O_3$ sample having $x = 0.037$, along with its associated point-by-point fit (pbp) for three different angles of incidence Φ.

be the main source of error, since instrumental error is small in comparison. Cross-sectional observation of the samples by TEM (Fig. 2) revealed that the films contain two main parts. The main part of the films, of thickness d, shows a uniform contrast. On the other hand, the upper part, of thickness r, exhibits a non-uniform contrast, which slowly decays toward the surface. We can rule out sample preparation damage as a potential reason for this feature, as there is still a thick (several hundreds nm) Pt layer to protect the top surface of the foil, plus damage was prevented by using low voltage ion beams at the end of the preparation. Such variation, in contrast, could have various and compounded origins, such as topographical roughness as well as variations in material crystallinity and density—for example, previous reports have shown for $x = 0.0$ that while the film was in the α-phase, the near-surface region contained α-, ϵ-, and amorphous Ga_2O_3.[37] Astonishingly, the results for the sum $(d + r)$ of thickness and roughness agree very well for both methods, especially for the samples

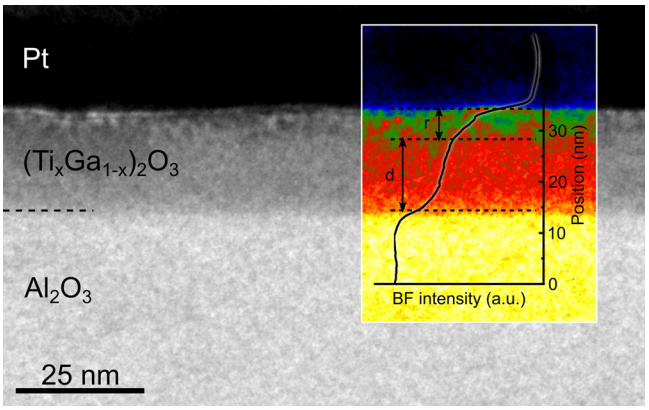

FIG. 2. BF-TEM cross-sectional view of the sample with $x = 0.053$. The inset is the same image but displayed with a temperature color-scale to highlight the change in contrast across the film.

$x = 0$, 0.037, and 0.053, which are those having a corundum-like crystal structure according to XRD. This shows that even for such thin samples, the ellipsometric method using Fabry–Pérot oscillations and an EMA layer for the roughness provides excellent results for thin film sample thicknesses. The roughnesses r, being in the same order of magnitude in ellipsometry and TEM, are clearly much higher than the ones obtained from atomic force microscopy.[31] However, this is not surprising, since the EMA roughness layer, as an optical roughness, also takes into account contaminants on the surface or surface band-bending. It is noticeable that the $x = 0.61$ sample is the only sample with more roughness than thickness in ellipsometry on the one hand and, on the other hand, the sample with the biggest deviation between ellipsometry and TEM thickness (d + r). This is, in our view, an indicator that this sample is becoming "porous" on the top since the roughness modeled with an EMA layer is filling the α-$(Ti_xGa_{1-x})_2O_3$ layer partly with void. However, this should, in general, not be a problem for determining the DF because in the evaluation process, it is possible to differentiate between effects that originate from layer thickness or roughness on the experimental data and the dielectric function itself, since these different parameters influence the modeling process differently, especially with three different angles of incidence measured.

The resulting pbp-DFs for all six samples are shown in Fig. 3. In ε_2, we find the absorption onset related to the first direct band-to-band transitions of the indirect α-Ga_2O_3, lowered by Coulomb interaction, i.e., excitonic effects. The pbp-DF of the $x = 0$ sample (Fig. 3, red curve) is in agreement with previous DFs of α-Ga_2O_3.[20,21,38–40] There are, however, some slight deviations to the literature DFs, which mainly originate from the fact that an isotropic model was used here. This makes sense not only because of, as explained earlier, film thickness and different angles of incidence measured, but also because it is unclear how the extraordinary DF would change with increasing Ti content, as we only have c-plane samples. However, this produces slight errors in broadening and amplitude, which are mainly responsible for this small deviations to the literature,[20,21,38,40] since these are

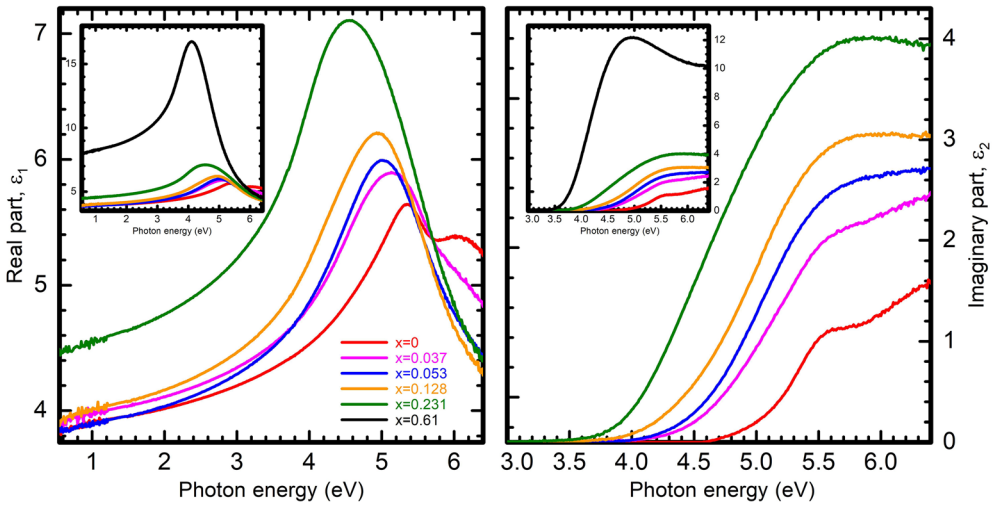

FIG. 3. Point-by-point (pbp) dielectric functions (DFs) of α-$(Ti_xGa_{1-x})_2O_3$ in the visible and ultraviolet spectral range, alloyed from $x = 0$ to $x = 0.231$. The real part ε_1 is shown on the left and the imaginary part ε_2 on the right. The inset again shows the same pbp-DFs, supplemented by the result from the $x = 0.61$ sample.

based on anisotropic models. With increasing Ti content, a red shift of the absorption onset and the corresponding peak in ε_1 is visible. This is related to the fact that both α-Ti_2O_3 and TiO_2, in several polymorphs, have a significantly smaller bandgap than α-Ga_2O_3, which has, like mentioned above, its indirect gap at about 5.0–5.4 eV[17–19] and the first direct gap at $\approx$ 5.6 eV.[20,21] The bandgap of α-Ti_2O_3, as a narrow-bandgap semiconductor or semi-metal, is found at 0–0.1 eV,[12–16] and the ones for anatase, brookite, and rutile TiO_2 are reported to be 3.4,[41] 3.27,[42] and 3.06 eV,[43] respectively. Thus, it is expected that the first direct transition as well is red shifted for Ti containing oxides compared to α-Ga_2O_3. On the other hand, in addition to the red shift, there is a clear increase in amplitude with increasing Ti content in both ε_1 and ε_2. This fits to the dielectric functions of rutile-,[44] anatase-,[45] and brookite-TiO_2,[46] which all show significant higher amplitudes in the dielectric functions, compared to Ga_2O_3. Looking at the density-of-states (DOS) of corundum-like α-Ti_2O_3 (Fig. 1 in Ref. 47), it shows that the upper valence band (VB) and the conduction band (CB) mainly consist of the Ti 3d-states and only little of the O 2p-states in contrast to the VB or CB of α-Ga_2O_3, which is dominated by Ga 4s- and 4p-states.[19] Between the lower VB in α-Ti_2O_3 and the VB in α-Ga_2O_3, there is no significant difference. Both DOS consist mainly of O 2p-states. Since the DF relates to the joint density-of-states, we understand that the partly filled and unfilled d-states of Ti are responsible for the massive amplitude increase in the DF of Ti_2O_3 as well as in the DF of the different TiO_2 polytypes, and the alloys of Ga_2O_3 with Ti. Other than in Ga_2O_3, it is expected that for Ti_2O_3, the upper VB near the Fermi level is not completely filled due to the small bandgap of 0–0.1 eV. Also, the comparable metal oxide V_2O_3 ($E_g < 1$ eV[48]) whose upper VB and CB DOS show a domination of V 3d-states as well likewise has a significantly higher $\varepsilon(\hbar\omega)$ amplitude, at the absorption onset, than Ga_2O_3.[49–51]

VB spectra from XPS measurements are displayed in Fig. 4. (Note that the wide scans are also shown, in a supplementary material (Fig. S3) together with further explanations regarding the XPS results.) It can be stated that the $x = 0$ spectra agree well with α-Ga_2O_3 literature,[52] as does the $x = 0.61$ sample to α-Ti_2O_3 by Chang *et al.*[53] Increasing Ti content and decreasing Ga can be seen in the wide scans (Fig. S3, Ti 2p and Ga 3d peaks) and reflected in the VB spectra with Ga 4s and 3d peaks at binding energies of $\sim$ 9 and 4 eV.[52] Also based on the wide scans in Fig. S3, there is a simplified quantification of Ti and Ga listed in Table I. Carbon and oxygen have been removed, and Ti 2p and Ga 3p peaks have been used to estimate the alloy composition. This fits reasonable to the RBS data from Barthel *et al.*,[31] just the $x = 0.61$ sample has a considerably deviance of over 10%. Regarding the VB spectra, it is important to note here that they were taken separately to the wide scans and with no charge reference peak (e.g., C 1s), so we can only estimate their position based on a photoelectron spectra taken previously and align to the VB in the wide scans. The VB spectra were acquired under the same conditions as the spectra, so this is reasonable. Because of the uncertainty in the charge state of the surface, we are cautious of attributing any trend to the peak positions in the VB, but since no obvious shift of the VB edge is detectable, we argue that since the absorption onset from ellipsometry, i.e., the

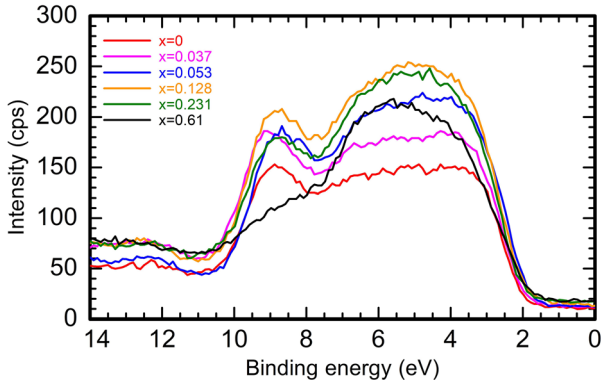

FIG. 4. XPS valence band spectra of α-$(Ti_xGa_{1-x})_2O_3$, alloyed from $x = 0$ to $x = 0.61$, aligned to the VB in the wide scans (Fig. S1).

fundamental direct transition does shift strongly with increasing Ti content, mainly the CB lowers. This fits to the fact that the VB DOS mainly consists of the O shells,[19,47] while CB DOS mainly consists of Ga shells,[19] being replaced with Ti d-shells with increasing x.[47]

In conclusion, we presented ultraviolet spectroscopic ellipsometry results on α-$(Ti_xGa_{1-x})_2O_3$ samples, grown by ALD, yielding the dielectric functions (DFs), along with transmission electron microscopy (TEM) and x-ray photoelectron spectroscopy (XPS). The layer thicknesses determined by ellipsometry are well confirmed by the TEM measurements. In the imaginary parts of the DFs, we find a clear redshift of the absorption onsets, along with a massive amplitude increase with increasing Ti content. We associate this amplitude increase with a domination of Ti 3d-states in the density-of-states. Ellipsometry and valence band XPS results led to the conclusion that mainly, the conduction band lowers with increasing Ti content and less the valence band.

See the supplementary material for a comparison of the Kramers–Kronig fulfilling model dielectric functions used as starting point for the point-by-point fit and the found point-by-point dielectric functions itself. Based on the absorption onset of this dielectric functions, the shift of the absorption onset vs Ti content is displayed. Furthermore, we provide a table with the uncertainties of the thicknesses and roughnesses from ellipsometry and TEM for all samples. At last, the XPS wide scans that have been obtained are shown.

This work was funded in part by the Leibniz Science Campus GraFOx II. The authors acknowledge the support from the Engineering and Physical Sciences Research Council (Nos. EP/R025282/1 and EP/S021434/1). EPSRC grant for the Kratos LiPPS XPS instrument no. EP/K005138/1.

AUTHOR DECLARATIONS

Conflict of Interest

The authors have no conflicts to disclose.

Author Contributions

Elias Kluth: Data curation (equal); Formal analysis (equal); Investigation (equal); Methodology (equal); Visualization (equal); Writing – original draft (lead). **Michael W. Fay:** Data curation (equal); Formal analysis (equal); Investigation (equal); Visualization (equal); Writing – review & editing (supporting). **Christopher Parmenter:** Investigation (equal). **Joseph William Roberts:** Formal analysis (equal); Investigation (equal); Methodology (equal). **Emily Smith:** Data curation (equal); Formal analysis (equal); Methodology (equal); Visualization (equal); Writing – original draft (supporting). **Craig T. Stoppiello:** Data curation (equal); Investigation (equal). **F. C-P. Massabuau:** Conceptualization (equal); Project administration (equal); Resources (equal); Supervision (equal); Visualization (supporting); Writing – review & editing (equal). **Rüdiger Goldhahn:** Funding acquisition (equal); Project administration (equal); Resources (equal); Supervision (equal). **Martin Feneberg:** Conceptualization (lead); Funding acquisition (equal); Project administration (lead); Resources (equal); Supervision (equal); Writing – review & editing (lead).

DATA AVAILABILITY

The data that support the findings of this study are available from the corresponding author upon reasonable request.

REFERENCES

[1]S. J. Pearton, J. Yang, P. H. Cary, F. Ren, J. Kim, M. J. Tadjer, and M. A. Mastro, Appl. Phys. Rev. **5**, 011301 (2018).
[2]P. K. Dasgupta, Q. Li, H. Temkin, M. H. Crawford, A. J. Fischer, in A. A. Allerman, K. H. A. Bogart, and S. R. Lee, in Fourth International Conference on Solid State Lighting, edited by I. T. Ferguson, N. Narendran, S. P. DenBaars, and J. C. Carrano, 2004 [Proc. SPIE **5530**, 174–181 (2004)].
[3]M. Higashiwaki, K. Sasaki, H. Murakami, Y. Kumagai, A. Koukitu, A. Kuramata, T. Masui, and S. Yamakoshi, Semicond. Sci. Technol. **31**, 034001 (2016).
[4]X. Hou, Y. Zou, M. Ding, Y. Qin, Z. Zhang, X. Ma, P. Tan, S. Yu, X. Zhou, X. Zhao *et al.*, J. Phys. D **54**, 043001 (2020).
[5]H. Xue, Q. He, G. Jian, S. Long, T. Pang, and M. Liu, Nanoscale Res. Lett. **13**, 290 (2018).
[6]S. Fujita and K. Kaneko, in Proceedings of 17th International Conference on Crystal Growth and Epitaxy (ICCGE-17), 2014 [J. Cryst. Growth **401**, 588 (2014)].
[7]H. Ito, K. Kaneko, and S. Fujita, Jpn. J. Appl. Phys., Part 1 **51**, 100207 (2012).
[8]M. Hilfiker, U. Kilic, M. Stokey, R. Jinno, Y. Cho, H. G. Xing, D. Jena, R. Korlacki, and M. Schubert, Appl. Phys. Lett. **121**, 052101 (2022).
[9]R. Cuscó, T. Yamaguchi, E. Kluth, R. Goldhahn, and M. Feneberg, Appl. Phys. Lett. **121**, 062106 (2022).
[10]S.-D. Mo and W. Y. Ching, Phys. Rev. B **51**, 13023 (1995).
[11]N. F. Mott, J. Phys. **42**, 277 (1981).
[12]J. M. Honig, Rev. Mod. Phys. **40**, 748 (1968).
[13]J. B. Goodenough, Prog. Solid State Chem. **5**, 145 (1971).
[14]L. F. Mattheiss, J. Phys.: Condens. Matter **8**, 5987 (1996).
[15]Y. Guo, S. J. Clark, and J. Robertson, J. Phys.: Condens. Matter **24**, 325504 (2012).
[16]Y. Li, Y. Weng, X. Yin, X. Yu, S. R. S. Kumar, N. Wehbe, H. Wu, H. N. Alshareef, S. J. Pennycook, M. B. H. Breese *et al.*, Adv. Funct. Mater. **28**, 1705657 (2018).
[17]J. Roberts, P. Chalker, B. Ding, R. Oliver, J. Gibbon, L. Jones, V. Dhanak, L. Phillips, J. Major, and F.-P. Massabuau, J. Cryst. Growth **528**, 125254 (2019).
[18]D. Shinohara and S. Fujita, Jpn. J. Appl. Phys., Part **47**, 7311 (2008).
[19]J. Furthmüller and F. Bechstedt, Phys. Rev. B **93**, 115204 (2016).
[20]M. Feneberg, J. Nixdorf, M. D. Neumann, N. Esser, L. Artús, R. Cuscó, T. Yamaguchi, and R. Goldhahn, Phys. Rev. Mater. **2**, 044601 (2018).
[21]M. Kracht, A. Karg, M. Feneberg, J. Bläsing, J. Schörmann, R. Goldhahn, and M. Eickhoff, Phys. Rev. Appl. **10**, 024047 (2018).
[22]K. Yoshimatsu, H. Kurokawa, K. Horiba, H. Kumigashira, and A. Ohtomo, APL Mater. **6**, 101101 (2018).
[23]Y. Li, Y. Yang, X. Shu, D. Wan, N. Wei, X. Yu, M. B. H. Breese, T. Venkatesan, J. M. Xue, Y. Liu *et al.*, Chem. Mater. **30**, 4383 (2018).
[24]Y. Li, Y. Zhu, M. Wang, M. Zhao, J. Xue, J. Chen, T. Wu, and S. A. Chambers, Adv. Funct. Mater. **32**, 2203491 (2022).
[25]N. Hasegawa, K. Yoshimatsu, D. Shiga, T. Kanda, S. Miyazaki, M. Kitamura, K. Horiba, and H. Kumigashira, Phys. Rev. B **105**, 235137 (2022).
[26]Z. Zhang, Z. Ding, X. Guo, Z. Luo, J. Wei, C. Yang, Y. Huang, and Z. Li, Mater. Res. Express **6**, 105920 (2019).
[27]B. Wang, D. Look, and G. Farlow, J. Phys. D. **53**, 444001 (2020).
[28]W. Mu, Z. Jia, G. Cittadino, Y. Yin, C. Luperini, Q. Hu, Y. Li, J. Zhang, M. Tonelli, and X. Tao, Cryst. Growth Des. **18**, 3037 (2018).
[29]W. Liu, X. Zhu, J. He, Y. Yang, T. Huang, X. Chen, and R. Zhang, Phys. Status Solidi RRL **15**, 2100411 (2021).
[30]A. Dakhel, Solid State Sci. **20**, 54 (2013).
[31]A. Barthel, J. Roberts, M. Napari, M. Frentrup, T. Huq, A. Kovács, R. Oliver, P. Chalker, T. Sajavaara, and F. Massabuau, Micromachines **11**, 1128 (2020).
[32]I. H. Malitson, J. Opt. Soc. Am. **52**, 1377 (1962).
[33]D. A. G. Bruggeman, Ann. Phys. **421**, 160 (1937).
[34]S. Shokhovets, L. Spieß, and G. Gobsch, J. Appl. Phys. **107**, 023509 (2010).

[35]G. Rossbach, M. Feneberg, M. Röppischer, C. Werner, N. Esser, C. Cobet, T. Meisch, K. Thonke, A. Dadgar, J. Bläsing *et al.*, Phys. Rev. B **83**, 195202 (2011).
[36]R. Schmidt, B. Rheinländer, M. Schubert, D. Spemann, T. Butz, J. Lenzner, E. M. Kaidashev, M. Lorenz, A. Rahm, H. C. Semmelhack *et al.*, Appl. Phys. Lett. **82**, 2260 (2003).
[37]J. Roberts, J. Jarman, D. Johnstone, P. Midgley, P. Chalker, R. Oliver, and F.-P. Massabuau, J. Cryst. Growth **487**, 23 (2018).
[38]P. Ning, J. Grümbel, J. Bläsing, R. Goldhahn, D.-W. Jeon, and M. Feneberg, Semicond. Sci. Technol. **35**, 095001 (2020).
[39]A. Segura, L. Artús, R. Cuscó, R. Goldhahn, and M. Feneberg, Phys. Rev. Mater. **1**, 024604 (2017).
[40]M. Hilfiker, R. Korlacki, R. Jinno, Y. Cho, H. G. Xing, D. Jena, U. Kilic, M. Stokey, and M. Schubert, Appl. Phys. Lett. **118**, 062103 (2021).
[41]H. Tang, F. Lévy, H. Berger, and P. E. Schmid, Phys. Rev. B **52**, 7771 (1995).
[42]A. Mattsson and L. Österlund, J. Phys. Chem. C **114**, 14121 (2010).
[43]J. Pascual, J. Camassel, and H. Mathieu, Phys. Rev. B **18**, 5606 (1978).
[44]T. E. Tiwald and M. Schubert, Proc. SPIE **4103**, 19–29 (2000).
[45]G. E. Jellison, L. A. Boatner, J. D. Budai, B.-S. Jeong, and D. P. Norton, J. Appl. Phys. **93**, 9537 (2003).
[46]M. Landmann, E. Rauls, and W. G. Schmidt, J. Phys.: Condens. Matter **24**, 195503 (2012).
[47]V. Singh and J. Pulikkotil, J. Alloys Compd. **658**, 430 (2016).
[48]Y. Guo, S. J. Clark, and J. Robertson, J. Chem. Phys. **140**, 054702 (2014).
[49]J. F. Mattheiss, J. Phys.: Condens. Matter **6**, 6477 (1994).
[50]M. M. Qazilbash, A. A. Schafgans, K. S. Burch, S. J. Yun, B. G. Chae, B. J. Kim, H. T. Kim, and D. N. Basov, Phys. Rev. B **77**, 115121 (2008).
[51]Y.-R. Park and K.-J. Kim, J. Korean Vac. Soc. **15**, 534 (2006); available at https://koreascience.kr/article/JAKO200601919973769
[52]J. E. N. Swallow, C. Vorwerk, P. Mazzolini, P. Vogt, O. Bierwagen, A. Karg, M. Eickhoff, J. Schörmann, M. R. Wagner, J. W. Roberts *et al.*, Chem. Mater. **32**, 8460 (2020).
[53]C. F. Chang, T. C. Koethe, Z. Hu, J. Weinen, S. Agrestini, L. Zhao, J. Gegner, H. Ott, G. Panaccione, H. Wu *et al.*, Phys. Rev. X **8**, 021004 (2018).